Atmos. Meas. Tech., 9, 5677–5698, 2016
www.atmos-meas-tech.net/9/5677/2016/
doi:10.5194/amt-9-5677-2016

Atmospheric Measurement Techniques
Open Access
EGU

Retrieval of absolute SO_2 column amounts from scattered-light spectra: implications for the evaluation of data from automated DOAS networks

Peter Lübcke[1], Johannes Lampel[1,2], Santiago Arellano[3], Nicole Bobrowski[1,6], Florian Dinger[1,2], Bo Galle[3], Gustavo Garzón[4], Silvana Hidalgo[5], Zoraida Chacón Ortiz[4], Leif Vogel[1,a], Simon Warnach[1,2], and Ulrich Platt[1]

[1]Institute of Environmental Physics, University of Heidelberg, Heidelberg, Germany
[2]Max Planck Institute for Chemistry (MPI-C), Mainz, Germany
[3]Department of Earth and Space Sciences, Chalmers University of Technology, Gothenburg, Sweden
[4]FISQUIM, Dirección de Laboratorios, Servicio Geológico Colombiano, Cali & Manizales, Colombia
[5]Instituto Geofísico, Escuela Politécnica Nacional, Quito, Ecuador
[6]Institute of Geosciences, Johannes Gutenberg University Mainz, Germany
[a]now at: Basque Centre for Climate Change (BC3), 48008, Bilbao, Spain

Correspondence to: Peter Lübcke (pluebcke@iup.uni-heidelberg.de)

Received: 26 January 2016 – Published in Atmos. Meas. Tech. Discuss.: 11 April 2016
Revised: 29 August 2016 – Accepted: 3 October 2016 – Published: 29 November 2016

Abstract. Scanning spectrometer networks using scattered solar radiation in the ultraviolet spectral region have become an increasingly important tool for monitoring volcanic sulfur dioxide (SO_2) emissions. Often measured spectra are evaluated using the differential optical absorption spectroscopy (DOAS) technique. In order to obtain absolute column densities (CDs), the DOAS evaluation requires a Fraunhofer reference spectrum (FRS) that is free of absorption structures of the trace gas of interest. For measurements at volcanoes such a FRS can be readily obtained if the scan (i.e. series of measurements at different elevation angles) includes viewing directions where the plume is not seen. In this case, it is possible to use these viewing directions (e.g. zenith) as FRS. Possible contaminations of the FRS by the plume can then be corrected by calculating and subtracting an SO_2 offset (e.g. the lowest SO_2 CD) from all viewing directions of the respective scan. This procedure is followed in the standard evaluations of data from the Network for Observation of Volcanic and Atmospheric Change (NOVAC). While this procedure is very efficient in removing Fraunhofer structures and instrumental effects it has the disadvantage that one can never be sure that there is no SO_2 from the plume in the FRS. Therefore, using a modelled FRS (based on a high-resolution solar atlas) has a great advantage. We followed this approach and investigated an SO_2 retrieval algorithm using a modelled FRS. In this paper, we present results from two volcanoes that are monitored by NOVAC stations and which frequently emit large volcanic plumes: Nevado del Ruiz (Colombia) recorded between January 2010 and June 2012 and from Tungurahua (Ecuador) recorded between January 2009 and December 2011. Instrumental effects were identified with help of a principal component analysis (PCA) of the residual structures of the DOAS evaluation. The SO_2 retrieval performed extraordinarily well with an SO_2 DOAS retrieval error of $1-2\times10^{16}$ [molecules cm^{-2}]. Compared to a standard evaluation, we found systematic differences of the differential slant column density (dSCD) of only up to ≈ 15 % when looking at the variation of the SO_2 within one scan. The major advantage of our new retrieval is that it yields absolute SO_2 CDs and that it does not require complicated instrumental calibration in the field (e.g. by employing calibration cells or broadband light sources), since the method exploits the information available in the measurements.

We compared our method to an evaluation that is similar to the NOVAC approach, where a spectrum that is recorded directly before the scan is used as an FRS and an SO_2 CD offset is subtracted from all retrieved dSCD in the scan to correct for possible SO_2 contamination of the FRS. The investigation showed that 21.4 % of the scans (containing significant amounts of SO_2) at Nevado del Ruiz and 7 % of the

scans at Tungurahua showed much larger SO_2 CDs when evaluated using modelled FRS (more than a factor of 2). For standard evaluations the overall distribution of the SO_2 CDs in a scan can in some cases indicate whether the plume affects all viewing directions and thus these scans need to be discarded for NOVAC emission rate evaluation. However, there are other cases where this is not possible and thus the reported SO_2 emission rates would be underestimated. The new method can be used to identify these cases and thus it can considerably improve SO_2 emission budgets.

1 Introduction

Since the introduction of the correlation spectrometer (COSPEC; Moffat and Millan, 1971; Stoiber et al., 1983) measurements of volcanic sulfur dioxide (SO_2) emission rates have become an additional tool for volcanologists to study the activity of volcanoes. More recently the availability of miniature spectrometers allowed the widespread application of the well-known differential optical absorption spectroscopy (DOAS) technique (e.g. Perner and Platt, 1979; Platt and Stutz, 2008) in volcanic environments (e.g. Galle et al., 2003; McGonigle et al., 2005; Elias et al., 2006). Automated systems for plume measurements were subsequently developed based on scanning the volcanic plume from different stationary positions: the so-called scanning-DOAS method (Edmonds et al., 2003). Scanning-DOAS instruments are now installed at many volcanoes in order to monitor SO_2 emission rates. The first installations of scanning-DOAS networks were done at Montserrat volcano (Edmonds et al., 2003). The Network for Observation of Volcanic and Atmospheric Change (NOVAC; Galle et al., 2010) is at present composed of more than 80 scanning-DOAS instruments at about 30 volcanoes worldwide. Furthermore, Mt. Etna and Stromboli, Italy, are both monitored by a comparable scanning-DOAS network (FLAME network; Burton et al., 2009; Salerno et al., 2009a). Another approach using similar instruments is the Hawaiian FLYSPEC fence line at Kilauea volcano which consists of 10 fixed, upward-looking spectrometers (Businger et al., 2015).

In order to correctly retrieve absolute SO_2 CDs from the recorded spectra via the DOAS method, and thus calculate accurate SO_2 emission rates, a background Fraunhofer reference spectrum (FRS), which is free of volcanic absorption features, is required. Typically, DOAS SO_2 evaluations use a FRS recorded in the scan (for example with a different viewing direction) to correct for the strong Fraunhofer lines of the solar spectrum. Contamination of this FRS with volcanic SO_2 absorption structures can in principle be corrected for by introducing an SO_2 CD offset that is subtracted from all SO_2 CDs of the respective scan (details about the calculation of this offset is provided in Sect. 2). However, if all viewing directions contain absorption signatures of volcanic SO_2, this approach leads to an incorrect offset and thus erroneous SO_2 CDs.

Therefore it is desirable to use a universal FRS, which is free of SO_2 (or in general free of the trace gas to be measured). First investigations on using a modelled background spectrum as an FRS for the DOAS evaluation of volcanic SO_2 were performed by Salerno et al. (2009b). Different implementations of this approach were used by Lübcke (2014) and Hibert et al. (2015) for evaluating NOVAC data collected at Nevado del Ruiz and at Piton de la Fournaise on Réunion island, respectively. Burton and Sawyer (2016) use a similar approach of modelling the background spectrum based on a high-resolution solar atlas for their iFit method, a direct fitting approach for the evaluation of volcanic SO_2 and BrO. This work will follow the idea of using a high-resolution solar atlas spectrum (we used the solar atlas by Chance and Kurucz, 2010) in order to calculate a gas-free background spectrum which is used as an FRS for the DOAS evaluation of SO_2.

The paper is structured in the following way. We applied the SO_2 retrieval with the modelled FRS to data from NOVAC in order to study how frequently differences between the standard evaluation and the approach using an artificial reference spectrum can be observed. In addition, we investigated the remaining residual structure of the DOAS evaluation with help of a principal component analysis (PCA). The results of the PCA were used in order to take instrumental effects into account and improve the retrieval. The evaluation process and possible pitfalls will be described in detail. We focussed on two large volcanic emission sources for our study: spectra were evaluated from two instruments at Nevado del Ruiz (Colombia), covering the time between January 2010 and June 2012, and from three instruments at Tungurahua (Ecuador), covering the time between January 2010 and December 2012.

The results of an evaluation using a modelled FRS were compared to a standard NOVAC evaluation, which uses a spectrum measured with an upward-looking viewing direction as FRS and subtracts an SO_2 offset to correct for possible contamination. Data from the NOVAC volcanoes Nevado del Ruiz and Tungurahua allowed us to determine how frequently all spectra from a particular scan of a scanning-DOAS instrument are contaminated with (volcanic) SO_2 absorption structures at these volcanoes. Additionally, it allowed us to investigate under which conditions scans occur with SO_2 absorptions present in all viewing directions.

2 Background spectra for scanning-DOAS instrument networks at volcanoes

DOAS (e.g. Perner and Platt, 1979; Platt and Stutz, 2008) is a well-established spectroscopic technique, based on Bouguer–Beer–Lambert's law, which uses the differential structures of molecules to remotely measure their slant col-

umn density (SCD) S. For sunlight measurements, an FRS $I_0(\lambda)$ is needed to remove the shape of the incident solar radiation, in particular the strongly structured Fraunhofer lines, and possible instrumental structures from the measurement. In this case, the evaluation procedure relies on the ratio of measurement spectrum $I(\lambda)$ and FRS. For one absorber, the optical depth τ is directly related to the absorption cross section $\sigma(\lambda)$ of the molecule and the SCD S of the measurement spectrum. However, in the case of a contaminated FRS the result only gives the difference in column density between measurement spectrum and the column density S_0 of the FRS:

$$\tau(\lambda) = -\ln\left(\frac{I(\lambda)}{I_0(\lambda)}\right) = -\ln\left(\frac{I_{\text{solar}}(\lambda)\times e^{-S\times\sigma(\lambda)}}{I_{\text{solar}}(\lambda)\times e^{-S_0\times\sigma(\lambda)}}\right) = \sigma(\lambda)\times(S-S_0). \quad (1)$$

The great advantage of the ratio method is that the highly structured solar Fraunhofer spectrum $I_{\text{solar}}(\lambda)$ is eliminated in the evaluation; the potential weakness is that it actually always determines the difference of two CDs, the so-called differential SCD (dSCD). This property also helps to eliminate potential stratospheric contributions to the trace gas column (if the solar zenith angle (SZA) is sufficiently constant between the measurement of $I(\lambda)$ and $I_0(\lambda)$); in addition, possible instrumental structures are also removed. However, one has to make sure by proper choice of $I_0(\lambda)$ that S_0 is negligible compared to S.

At volcanoes, during traverse measurements or campaign based scanning measurements a gas-free FRS $I_0(\lambda)$ is typically obtained by choosing a spectrum recorded with a viewing direction that is believed not to intersect the plume. However, the choice of FRS is more difficult for automatised scanning-DOAS networks, like NOVAC (Galle et al., 2010) or the FLAME network (Burton et al., 2009; Salerno et al., 2009a), since it is not always clear whether the FRS contains significant volcanic SO_2 absorption structures or not.

Galle et al. (2010) suggested for NOVAC to use a zenith-looking spectrum as FRS for the DOAS evaluation. Possible contamination of the FRS is taken into account during the evaluation by subtracting an offset SO_2 CD (that corresponds to $-S_0$) from the derived CD S. Based on preliminary tests on measurements at a few volcanoes, the authors suggested using the average of the lowest 20 % SO_2 CDs from the valid retrievals in each scan as the offset CD $-S_0$ but other options (e.g. using the lowest SO_2 CD obtained in a scan) are possible as well. The offset value is determined individually for each scan (i.e. recordings of spectra from one horizon to the other) and subtracted from all SO_2 CDs of the respective scan. However, if all spectra of one scan are influenced by SO_2 absorption (i.e. S_0 is not negligible compared to S) subtracting the offset will lead to an underestimation of the SO_2 CDs. Therefore, this approach can lead to a systematic underestimation of the SO_2 emission rate if SO_2 absorption structures are present at all viewing directions of the instrument.

For the FLAME network, Salerno et al. (2009b) investigated the use of a modelled background spectrum based on a high-resolution solar atlas for the DOAS evaluation of SO_2. The authors noted that wide volcanic plumes, which may cover the entire field of view of the instrument and prevent acquisition of a plume-free reference spectrum, are relatively frequently observed at Mt. Etna, Italy. The authors recorded spectra of calibration cells (with known SO_2 content) and tuned the parameters of the DOAS evaluation in order to reproduce the known SO_2 CD of the cells. This makes this approach rather labour intensive and it does not appear to be practical for instruments which are already installed at remote locations. In addition, Salerno et al. (2009b) used three different values for the full width at half maximum (FWHM) of the instrument line function (ILF) for the convolution of the different trace gas absorption cross sections and the convolution of the high-resolution solar atlas spectrum (i.e. the FWHM for the O_3 convolution was different from the FWHM for the SO_2 convolution). However, the ILF is an instrument property. While there are influences, e.g. variations of the FWHM over the detector or variations with instrument temperature, it does not depend on the trace gas itself, and therefore there is no physical reason to encounter three different FWHM values of the ILF.

In our new evaluation scheme, we followed the approach to model the FRS on the basis of a solar atlas instead of measuring it on site; the required instrumental properties are retrieved from the measurement data itself. We modelled the FRS I_0 by convolving the high-resolution solar atlas $I_K(\lambda)$ by Chance and Kurucz (2010) using the ILF as a convolution kernel $H(\lambda)$.

We used the same ILF for the convolution of the high-resolution solar atlas spectrum as well as for the convolution of all trace gas cross sections. Unfortunately there are only records of the ILF at room temperature available for most NOVAC instruments. This introduces an additional error source, since the ILF varies with instrument temperature (Pinardi et al., 2007). All reference cross sections were convolved using the 334.15 nm line of a mercury emission lamp which was recorded at room temperature as a convolution kernel.

In reality, the recorded signal due to the incident solar radiation is influenced not only by the spectral resolution of the spectrometer but also by the wavelength-dependent efficiency of the detector, the efficiency of the spectrometer's grating or the instrument's optical system. We combine these wavelength-dependent effects in a factor $Q(\lambda)$ (neglecting detector effects like offset and dark current, which were corrected beforehand) and describe a measured spectrum as

$$I_{0,\text{measured}}(\lambda) = (I_{\text{incident}}(\lambda)\times H(\lambda))\times Q(\lambda). \quad (2)$$

Only the high-frequency variations (in wavelength) of $Q(\lambda)$ need to be corrected for in the retrieval, since slow varia-

tions are eliminated by the high-pass filtering inherent to the DOAS. Burton and Sawyer (2016) additionally mentioned small variations between different pixels. In their paper, these variations are taken into account by characterising them with the help of a deuterium lamp (i.e. recording a so-called flat spectrum). Here we use a different approach and include the above mentioned wavelength-dependent effects $Q(\lambda)$ and the pixel-to-pixel variations as a pseudo-absorber in the DOAS retrieval. Assuming that $I_K(\lambda)$ is an ideal representation of the incident radiation $I_{\text{incident}}(\lambda)$ (i.e. $I_K(\lambda) = I_{\text{incident}}(\lambda)$) we are left with a wavelength-dependent residual structure when calculating the optical depth τ using Eqs. (1) and (2):

$$\tau = -\ln \frac{I_{0,\text{measured}}(\lambda)}{I_{0,\text{model}}(\lambda)} = -\ln Q(\lambda). \quad (3)$$

Two pseudo-absorbers were included in the DOAS fit scenario in order to account for these instrumental effects. Information about these absorbers was obtained from the spectra themselves by using a PCA on the residuals from a DOAS fit for each instrument individually. We interpret the first principal component to be caused by detector effects as given by $Q(\lambda)$ in Eq. (3). Including the second principal component in the DOAS fit greatly improved the stability of the retrieval, in particular for the instruments installed at Tungurahua. This second principal component appears to account largely for variations of the instrument calibration and temperature-induced changes of instrument properties. However, the principal components could additionally contain structures from the Chance and Kurucz (2010) solar atlas as suggested by Burton and Sawyer (2016). This solar atlas is based on measured spectra synthesised from two different measurement platforms and corrected for atmospheric absorption lines.

3 Data evaluation

This section discusses the details of the SO_2 retrieval. A summary of the evaluation steps can be found in the Appendix.

3.1 Settings of the DOAS retrieval

All spectra were evaluated for SO_2 using the DOASIS software package (Kraus, 2006) with two different settings.

- Method A: an evaluation similar to the regular NOVAC evaluation. This method used a spectrum that was acquired by the instrument immediately before the scan with a scan angle of 0° as FRS (smallest deviation from the zenith direction; see Galle et al., 2010, for the exact definition of the scan angle). After evaluation of a complete scan through the sky, which means recording spectra from one horizon to the other horizon, an SO_2 CD offset was calculated and subtracted from all SO_2 CDs of the respective scan.
- Method B: an evaluation using a modelled background spectrum, based on a high-resolution solar atlas spectrum as an FRS. In this case the same FRS was used for the evaluation of all spectra from one instrument. The FRS was calculated on the basis of the Chance and Kurucz (2010) solar atlas by convolving the high-resolution solar atlas spectrum with the ILF of the respective spectrometer. First a DOAS evaluation using this fit scenario was performed to create a set of residual spectra which were analysed with help of a principal component analysis. In a second evaluation round the first two principal components were included in the fit scenario as pseudo-absorbers in order to account for instrumental effects (see Eqs. 2 and 3, above). The results of the second run were used in order to investigate the relative difference between the two methods.

As a first step before the DOAS fit, all spectra were corrected for dark current and offset by subtracting a dark spectrum, which is recorded using the same parameters (number of co-added spectra and exposure time) as the measurement spectra but with the telescope pointing to the ground, where the field of view of the spectrometer is blocked by a closed window of the scanner. Afterwards spectra that were under- or overexposed were removed from the evaluation. This was done in two steps: first we removed all spectra for which the highest exposure was below 12 or above 92 % of the maximum number of counts in the complete spectrum (500 and 3800 of 4096 counts, respectively, for a single exposure). These limits refer to spectra corrected for dark current and offset. Limiting the maximum exposure over the complete spectrum (not just the part used for SO_2 retrieval) served to prevent problems due to blooming effects. Second, after investigating the fit quality for both retrieval methods we additionally excluded all spectra with a maximum intensity below 5 or above 85 % in the SO_2 retrieval wavelength range from further processing. The latter maximum value was chosen since the χ^2 of the retrieval largely increased at higher intensities due to detector non-linearity.

After a wavelength calibration (by comparing the spectrum with the Fraunhofer lines of the Chance and Kurucz, 2010, solar atlas spectrum), spectra were evaluated for SO_2 using a DOAS fit. The DOAS evaluation was performed in the wavelength range between 310 and 326.8 nm. In order to create the principal components (for which the input vectors need to have the same length), we chose the channels corresponding to these wavelengths once at the beginning and kept the channels of the fit range fixed throughout the entire evaluation process.

Based on the respective FRS, a Ring spectrum was calculated and included in the fit in order to account for the Ring effect, the filling of the Fraunhofer lines of the solar spectrum (Shefov, 1959; Grainger and Ring, 1962). The Ring spectrum is calculated using a method that is implemented in DOASIS, which is based on Bussemer (1993).

The DOAS fit approach was (except for the FRS and the additional pseudo-absorbers) identical for methods A and B:

to account for trace gas absorption in the atmosphere one SO_2 cross section (recorded at 298 K by Vandaele et al., 2009) and two O_3 cross sections (recorded at 221 and 273 K by Burrows et al., 1999) were included in the DOAS fit. The 334.15 nm peak of a mercury line spectrum recorded at room temperature was used as a representation of the ILF for the convolution. The O_3 cross section with a temperature of 273 K was orthogonalised with respect to the lower temperature O_3 cross section in the DOASIS software. To account for small inaccuracies in the wavelength calibration, the FRS and the Ring spectrum as one set and all trace gas reference cross sections as another set were allowed a wavelength shift and squeeze with respect to the measurement spectrum for Method A. A shift of ± 0.2 nm was allowed and the spectra were allowed to be stretched/squeezed by ± 2 %. Since the modelled FRS spectrum (Method B) is synthetic, the calibration is inherited from the solar atlas. Given the stated accuracy of the calibration of the solar atlas $\leq 3.2 \times 10^{-4}$ nm (Chance and Kurucz, 2010), we assume that it is correct for our purposes. Therefore the FRS, the Ring spectrum and all trace gas absorption cross sections were only allowed to be shifted and squeezed as one set in Method B. Some of the instruments had a "hot detector pixel", a pixel which always showed a much higher signal. For Method A this was not a problem, since a similar signal is typically found in the FRS. To exclude these hot pixels from the fit in Method B an additional absorber that is zero everywhere except at the location of the hot pixel (where its value was chosen as 1) was included in the fit. A DOAS polynomial of third order was used to remove broadband variations in the spectrum. In order to take a possibly remaining offset into account (after the dark spectrum removal, for example due to instrumental stray light), an additional constant in intensity space was allowed in the retrieval.

After an initial DOAS fit the retrieved trace gas CDs were used as input parameters for a saturation correction and the I_0 correction of the SO_2 and the O_3 absorption cross sections. Both the I_0 effect (for highly structured light sources) and the saturation effect (for absorbers with high optical densities) are due to narrow structures that cannot be resolved by the spectrometer and the fact that the exponential function in the Bouguer–Beer–Lambert law and the convolution do not commute (Wenig et al., 2005). The correction of both effects are standard procedures in DOAS evaluations (Platt et al., 1997; Platt and Stutz, 2008). Both O_3 cross sections were corrected for the saturation effect using the CD of the (non-orthogonalised) O_3 cross section recorded at 221 K.

3.2 Calculation of the SO_2 offset value for Method A

As discussed above, it cannot be ruled out that the spectrum used as FRS in Method A is contaminated with SO_2. One approach to (partially) correct for this contamination is to calculate an SO_2 offset value. This value is calculated for each scan and subtracted from all SO_2 CDs of the respective scan. Deviating from the approach of Galle et al. (2010), we used the lowest SO_2 CD of each scan as the SO_2 CD offset instead of using the average over the SO_2 CD of several spectra. As the offset value is based on only one single spectrum it is important to remove spectra where the SO_2 fit failed completely from the results before calculating the offset value.

We therefore only used viewing directions that were not influenced by obstacles in the field of view and where the intensity was adequate, for further evaluation. This meant, for example, that for instrument D2J2201 at Nevado del Ruiz only spectra with a scanning angle between -72 and 86° were allowed (the scan angle is defined from -90 to $+90$° clockwise for an observer looking from the instrument towards the volcano). If no viewing directions influenced by obstacles were identified, we only excluded the two lowest viewing directions for these instruments (i.e. scan angle of ± 90°). Limiting the viewing directions for the calculation of the offset is a trade-off. Viewing directions with obstacles (for example mountains or buildings) in the field of view obviously lead to erroneous DOAS fit results. However, excluding too many viewing directions could influence the results, since we might in some cases exclude viewing directions which are interference free.

We also removed spectra from further evaluation, where the DOAS fit from Method A clearly failed and had a χ^2 above 0.05. χ^2 was calculated for all pixels of the evaluation range and typically had values between 1×10^{-3} and 0.01. Therefore, this threshold only removed a small fraction below 1 % of the remaining spectra from further evaluation. Afterwards the lowest SO_2 CD of each scan was chosen as the offset value and subtracted from all SO_2 CDs of the respective scan.

3.3 Principal component analysis for Method B

PCA (Pearson, 1901; Smith, 2002) is a statistical technique that can be used to transform a set of vectors (in our case the remaining residual structure of the DOAS fit) into a set of orthogonal vectors and also provides immediately time series for the magnitude of each of the vectors. These orthogonal vectors are chosen in such a way that a sequence of n principal components provides the best possible linear approximation of the residual data using an euclidean norm (Hastie et al., 2001). The PCA technique was first applied in DOAS applications by Ferlemann (1998). Li et al. (2013) retrieved SO_2 from OMI satellite data with help of PCA. The PCA was used by Lampel (2014) to identify problems in the spectral evaluation of multi-axis DOAS and cavity-enhanced DOAS measurements. We performed a PCA on the residuals of the initial DOAS fit with the modelled FRS in order to take instrumental effects into account (see Eq. 3). Different from usual PCA applications, we did not remove the mean value from the spectra since we are interested in all systematic variations of the residual spectra from the zero value (which would be the ideal case).

In order to find mainly instrumental effects and exclude other problems in the residuals (e.g. large O_3 CDs, objects in the light path), even more restrictive criteria had to be fulfilled by the spectra included in the PCA:

- Only spectra with a scan angle in the range of −75 to +75° were included in order to avoid influences by very long atmospheric light paths and errors due to topographic features or buildings/vegetation in the light path.
- Only spectra recorded at SZAs below 60° were used, to exclude spectra with large stratospheric O_3 CDs.
- Only spectra with a χ^2 below 0.01 for Method A (using a spectrum recorded with the same instrument before the scan as FRS) were included in order to exclude spectra that are already problematic in a regular DOAS retrieval.
- A more restrictive selection criterion for the intensity of the spectrum was chosen. Only spectra with a maximum number of counts between 32 and 78 % (1333 or 3200 counts for a single exposure after dark current correction) of the maximum possibly number of counts over the entire spectrum were allowed for the PCA.
- Only spectra that were not influenced by SO_2 (i.e. SO_2 CD below two times the DOAS retrieval error) were allowed for the PCA. This was assured by a DOAS fit using a modelled spectrum as FRS without including additional PCA pseudo-absorbers.

There are some pitfalls which can make the application of the PCA non-trivial. The spectra that are analysed in the PCA should not include any real SO_2 absorption features because this would introduce a potential negative SO_2 offset. These features would show up in the residual structure and thus influence the principal components and ultimately lead to unreliable fit results. Li et al. (2013) assured this criterion by selecting an SO_2-free reference sector. For our data set we have to use a different approach to only select spectra without SO_2 structures for the PCA. We chose spectra from times with only little degassing activity to create the PCA. Since this was difficult (in particular at Nevado del Ruiz) rather than relying on guesses about the SO_2 CD we used an additional SO_2 fit with a modelled FRS to select gas-free spectra. Only spectra where the absolute value of the SO_2 CD was smaller than twice the DOAS fit error were considered in the PCA. Using a similar argument, including an SO_2 absorption cross section in the DOAS fit used for the PCA can lead to problems. Inaccuracies in the DOAS fit with a modelled FRS (due to the same detector structures that we want to find with help of the PCA) might lead to a false SO_2 signal (with positive or negative sign). The fit might find these structures and thus remove them from the residual spectrum. Thus they are missing in the principal component which is later included in the DOAS fit. In this case the principal component would not only describe the instrumental effects but also add/subtract SO_2 features from the spectrum and thus lead to an additional error of the SO_2 CD. It is therefore crucial not to include SO_2 in the DOAS fit that is used to create the residual structures that are investigated with help of the PCA. Therefore, we made two DOAS fits with the modelled FRS. The first fit had an SO_2 absorption cross sections included and was used to select spectra suited for the PCA. The second fit did not include an SO_2 absorption cross sections and was used to create the residuals.

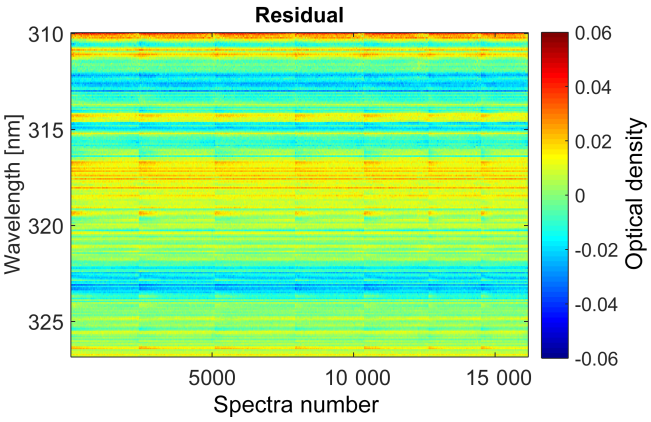

Figure 1. Time series of the residuals optical density (colour-coded) of a DOAS retrieval using a modelled background spectrum. The figure shows data from the 7 days (5–11 September 2010) used in the PCA (without SO_2 included in the fit) for instrument D2J2201 at Nevado del Ruiz. The residuals are shown in chronological order. The discontinuities in horizontal direction are at the transition from one day to another.

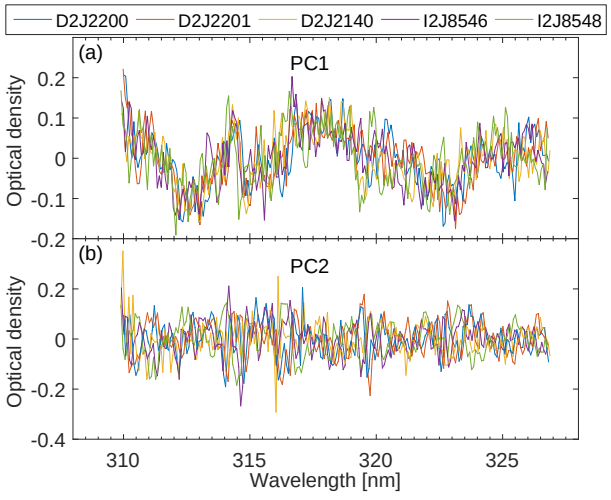

Figure 2. The first two principal components that were included in the solar atlas evaluation shown for all five instruments at Nevado del Ruiz and Tungurahua. For Tungurahua the principal components from 2010 are shown.

At Nevado del Ruiz we selected 7 days in September/October of 2010 as our training data set for the PCA; the increasing activity after this time made it difficult to find gas-free days. At Tungurahua the situation was quite different: the volcano had periods of higher activity alternating with times with very low or no degassing at all. The instruments at Tungurahua also showed a drift of instrument calibration and we thus performed the PCA for each year individually. For each instrument and each year at Tungurahua we chose 10 days as our training data for the PCA. These 10 days were distributed over the year (at times of low volcanic degassing activity) in order to find long-term variations of the principal components. For example in 2009 we chose 5 days in January and 5 days in October for the PCA. For each PCA (that means one for each instrument at Nevado del Ruiz and one per instrument and per year at Tungurahua) typically more than 10 000 residual spectra were evaluated. Choosing only a small set of a few days for the PCA has several advantages. For one, it allows us to investigate the performance on gas-free days that are not part of the training data. Using all gas-free days for the PCA would by definition shift the average SO_2 CD to zero on these days. The second advantage is of a more practical nature; in real life it is not always feasible to manually investigate a large amount of data to find gas-free days, and only a few days have to be sufficient.

4 Results

At Nevado del Ruiz the two original stations, Bruma (instrument D2J2200, installed at a 3100 m distance from the crater in NW direction) and Alfrombales (instrument D2J2201, installed at 4150 m distance in W direction from the crater), have been installed in 2009. We evaluated spectra recorded between 1 January 2010 and 30 June 2012 from these two NOVAC stations (see Garzon et al., 2013, and Lübcke et al., 2014, for maps of the stations and more information on NOVAC measurements at Nevado del Ruiz). After evaluating the spectra, we found that the instrument's GPS antennas occasionally reported erroneous times, which led to offsets in the time stamps of spectra of up to 55 min. Before selecting spectra for the final results (Sect. 4.2–4.4), we corrected for possible time offsets with help of a Langley plot of the O_3 CDs (see Appendix A for details).

At Tungurahua there are currently four stations installed. A map of the different NOVAC stations at Tungurahua can be found in Galle et al. (2010) and additional information on the gas emissions from Tungurahua is available in Hidalgo et al. (2015). We used data recorded between January 2009 and December 2011 from the three stations that are located in the main wind direction: Pillate, 8000 m W, Huayarapata, 9100 m NW, and Bayushig, 11900 m SW of the volcano.

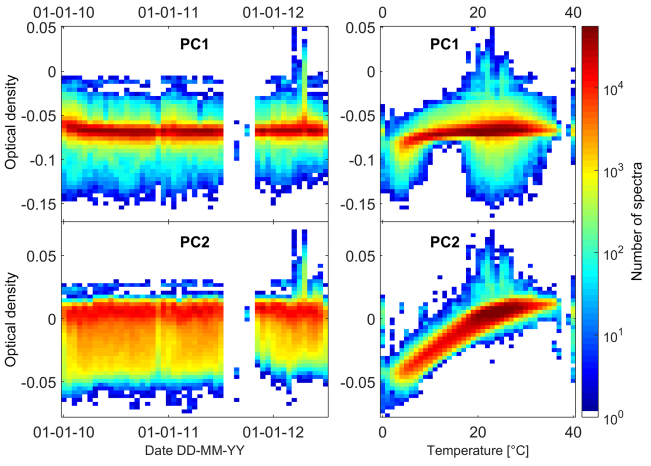

Figure 3. Peak-to-peak apparent optical density (e.g. peak-to-peak optical depth of the principal component times the fit coefficient) of the first and second principal components for instrument D2J2201 at Nevado del Ruiz. In the left column the principal components are shown as a function of time and in the right column as a function of instrument temperature. It appears that PC1 describes a constant apparent spectral feature of the instrument while PC2 describes a temperature-dependent effect.

4.1 Structure and variation of the principal components

A time series of the residual structures for the spectra used in the PCA for instrument D2J2201 is shown in Fig. 1. It can be clearly seen that there is a dominating constant structure apparent in all spectra. This residual structure is quite similar for all instruments, as can be seen from Fig. 2, which shows the first two principal components of the residual structures for all instruments included in this study. While the principal components are not exactly the same, similar broadband as well as narrowband features can be observed for all instruments, in particular for the first principal component.

At Nevado del Ruiz, we observed that the first principal component is mostly constant with only little temperature variations while the second principal component usually shows stronger temperature-dependent variations. This can be seen by looking at the peak-to-peak optical density of the first and second principal component, shown in Fig. 3 for instrument D2J2201. For a better comparison with other absorbers the apparent optical density of the respective principal component (i.e. the fit coefficient multiplied with the peak-to-peak optical density of the pseudo-absorber) is shown in Figs. 3 and 4.

The behaviour of the instruments at Tungurahua is more complex (see Fig. 4 for an example of instrument I2J8548). Both principal components show a time dependency for all three instruments at this volcano; a temperature dependency of the principal components can only be observed for some

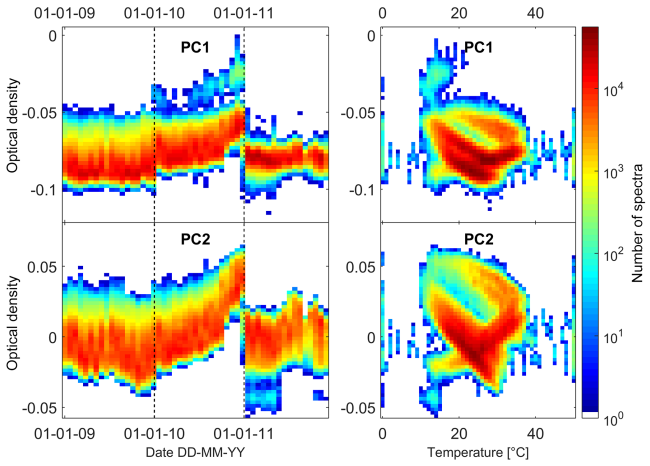

Figure 4. Peak-to-peak apparent optical density of the first and second principal components, as Fig. 3, but for instrument I2J8548 at Tungurahua. The vertical dashed lines indicate the start of the intervals for which a new set of principal components was calculated. In contrast to the case shown in Fig. 3 here both PC1 and PC2 show a temporal drift but a rather chaotic temperature dependence. It is interesting to note that the instruments at Tungurahua show behaviour similar to this figure, while both spectrometers at Nevado del Ruiz both show a behaviour similar to the one shown in Fig. 3

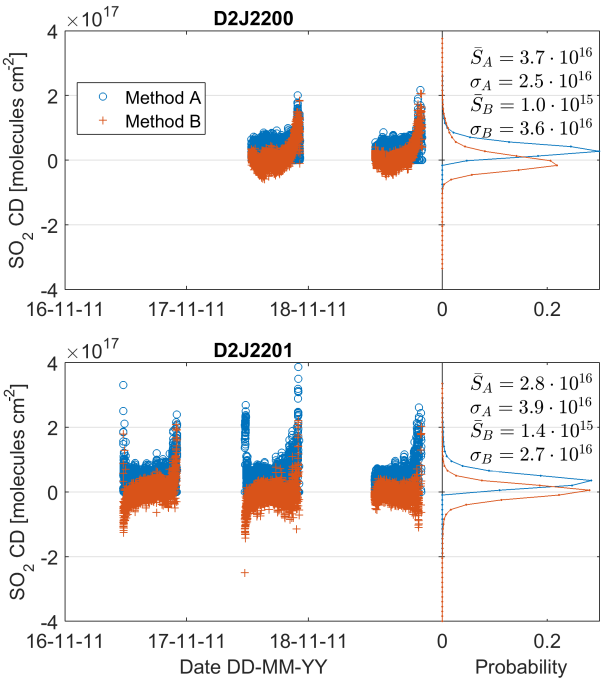

Figure 5. SO_2 column densities for days with presumably no SO_2 apparent in the light path for the two instruments at Nevado del Ruiz. The histogram on the right side shows the distribution of the values of both methods for all gas-free days in the data set. An increase in SO_2 CDs in the early morning and towards the evening can be observed. However, the histogram shows that this only influences a small fraction of the data (typically for SZAs above 70°).

of the instruments. The same kind of figure for the three other instruments can be found in the Appendix.

We interpret the first principal component as the factor $-\log(Q(\lambda))$ from Eq. (3), while the second principal component appears to take temperature-induced or time-dependent variations of the instrument into account.

4.2 Comparison of the SO_2 column densities from methods A and B

Before directly comparing the SO_2 CDs of the two methods, we first investigate how well Method B performs if there is no absorbing gas in the light path (i.e. if the retrieval yields zero when no gas is present). We assessed this by manually choosing gas-free days and looking at the distribution of the SO_2 CDs. Besides low SO_2 CDs from both Method A and B, another criterion to identify gas-free days are the variations of the SO_2 CDs within one scan, which are typically less structured if no gas is present. At Nevado del Ruiz fewer days (73 or 137 days for D2J2200 or D2J2201, respectively) were available in the entire data set due to strong activity. At Tungurahua more data were available, since periods with volcanic activity or no degassing both occur frequently. Examples of the diurnal variation of the SO_2 CDs for both instruments at Nevado del Ruiz during gas-free days are shown in Fig. 5. In contrast to the other instruments (at both volcanoes), instrument D2J2200 (Fig. 5 at the top) showed a clear variation of the SO_2 CD (as derived by Method B) over the course of a day with enhanced CDs during the evening. However, the histogram on the right-hand side (which was created for all gas-free days) shows that even though the increase towards the evening is clearly visible it only influences a very small fraction of the data set. The other instruments (an example is D2J2201 in Fig. 5, bottom) only show deviations from the zero value during the first or last scan of each day. At these times Method A shows larger variation within one scan as well. The average SO_2 CD for gas-free periods are between -7×10^{15} [molecules cm^{-2}] and 1.5×10^{15} [molecules cm^{-2}], with a standard deviation of 2.7–3.6 $\times10^{16}$ [molecules cm^{-2}]. The values of the mean SO_2 CD and the standard deviation for all instruments are given in Table A1 in the Appendix.

As discussed in detail below, the SO_2 CDs derived by Method B are frequently considerably larger than those derived by Method A. In order to study the ability of both methods to derive the variation of the SO_2 CD within one scan we compared the dSCDs by subtracting an offset from the data derived by Method B as well and plotted the result in Fig. 6, which shows a two-dimensional histogram of the SO_2 CDs from Method A (in y direction) and Method B (in x direction, after offset removal) for the complete data set (January 2010–June 2012) for instrument D2J2201 at Nevado del Ruiz. We used a bin size of 5×10^{16} [molecules cm^{-2}] (in x as well as in y direction); the colour denotes how often a certain SO_2

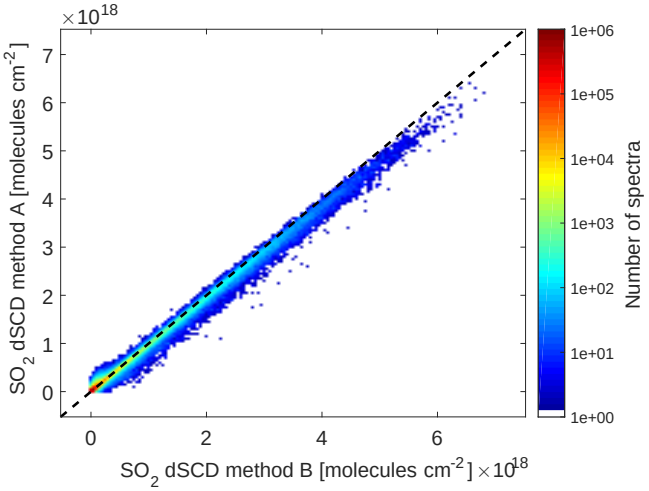

Figure 6. Two-dimensional histogram of the SO_2 SCDs from the solar atlas method vs. the SCDs from the NOVAC evaluation for instrument D2J2201 at Nevado del Ruiz. For this figure an offset value was subtracted from the solar atlas SO_2 CDs as well. The dSCDs of both methods show a good linear relationship with a slope close to 1 (0.956 in this case). The black-dashed line shows the identity line.

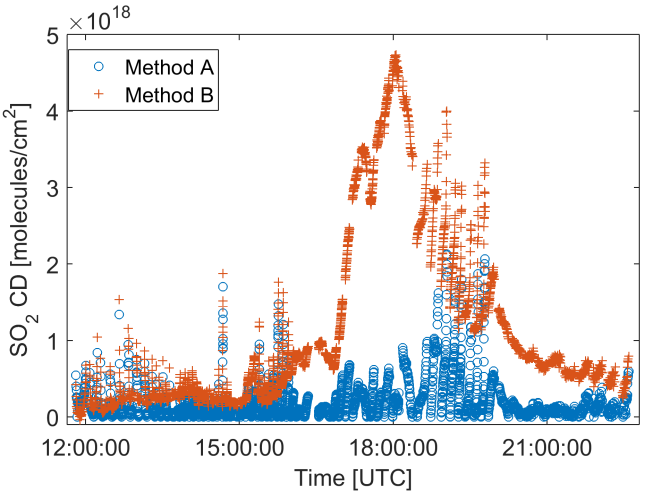

Figure 7. SO_2 CDs at Nevado del Ruiz on 6 March 2012 from instrument D2J2201. Method A (which is similar to the standard NOVAC approach) leads to much lower SO_2 CDs compared to Method B (modelled FRS). Many of the scans from this day would have been rejected by the standard NOVAC evaluation due to very low plume completeness values (see Galle et al., 2010, for details on plume completeness).

CD pair exists. The slope of this curve can be interpreted as the relationship between the dSCDs from the two methods. When an offset is removed for both methods, they show a linear relationship. The slope of this curve is not exactly unity, it varies between 0.88 and 1.14 for the different instruments (the values are given in Table A1 in the Appendix). It is not entirely clear, what causes the difference between the two methods. One possible explanation is that spectrometer stray light (that should be corrected for by an additional offset in intensity space during the fit) is not corrected for in the same way for Method A and B. While the measurement spectrum is the same for both methods, only the FRS of Method A is influenced by stray light while the FRS of Method B is not contaminated with stray light.

After making sure that Method B performs well for gas-free days and that both methods show similar SO_2 dSCDs (within a certain error), we trust that Method B works and compare the absolute SO_2 CDs from Method A with Method B. One rather extreme example of the difference between the SO_2 CDs derived for both methods is shown in Fig. 7. This figure shows data from instrument D2J2201 at Nevado del Ruiz recorded on 6 March 2012. It can be clearly observed that Method B retrieved much larger SO_2 CDs, especially during the middle of the day. At this time the modelled FRS leads to SO_2 CDs of up to 5×10^{18} [molecules cm^{-2}] while Method A only shows SO_2 CDs around 1×10^{18} [molecules cm^{-2}]. The variations within each scan (which can be identified by the small gaps between data points) show similar variations for both methods. However, for Method A each scan has one viewing direction with an SO_2 CD of 0, since we subtracted an offset value for each scan (see Sect. 3.2). Additional criteria exist for the calculation of SO_2 emission rates (e.g. the completeness value; see Galle et al., 2010, for an exact definition) that would have led to discarding most measurements on the day presented in Fig. 7.

We also observed days in which both methods agreed nicely. One example is 11 January 2012, as shown in Fig. 8. Only a part of the day is shown for a better visibility of the variability of the SO_2 CDs within each scan.

A more systematic way to compare the SO_2 CDs of many measurements is shown in the histogram in Fig. 9. This figure again shows 2-D histograms of the SO_2 CDs from Method A (in y direction) and Method B (in x direction, this time without removing an offset) for the complete data set (January 2010–June 2012) for instrument D2J2201 at Nevado del Ruiz. The same bin size as above was used. As can be seen in Fig. 9, Method B leads to larger SO_2 CDs on a significant number of spectra. When evaluated by Method A only a negligible number of spectra has larger SO_2 column densities than given by Method B. The larger SO_2 CDs of Method B are most likely caused by contamination of all viewing directions with SO_2 absorption structures (the likely reasons for the contamination will be discussed in Sect. 5).

4.3 Fit quality and SO_2 fit error for Method B

An example of an SO_2 fit using a modelled background spectrum is shown in Fig. 10. The spectral signature of SO_2 (SO_2 CD of 1.63×10^{17} [molecules cm^{-2}]) can be easily identified

in the fit. The residual is unstructured and has a peak-to-peak value of roughly 1.5×10^{-2}; this value is comparable to a regular DOAS SO_2 fit using an FRS measured with the same instrument from the same scan. Note that the first principal component was found in the fit extraordinarily well while the second principal component does not contribute to the spectrum significantly in this case, which is a spectrum recorded at 16.3 °C.

The time series of the SO_2 retrieval error (for instrument D2J2201) depicted in Fig. 11 shows a more or less constant distribution of the fit error between March 2010 and February 2012, the majority of spectra have an fit error below 2×10^{16} [molecules cm^{-2}]. Slightly larger fit errors can be observed in the beginning of 2010. Much larger SO_2 fit errors after March 2012 are caused by strong volcanic activity and large SO_2 CDs that lead to non-linearities in the DOAS retrieval (Method A shows increased retrieval errors in this period as well).

For instrument I2J8548 (as one example from Tungurahua) the SO_2 fit errors in Fig. 12 are slightly larger and show some temporal variation. There are larger values of the SO_2 fit error at the border between 2 years. This indicates that variations of the instrument's characteristics were not completely captured by the principal components. In these cases, performing the PCA on smaller time intervals can help to improve the performance.

The SO_2 DOAS fit error of Method B is shown as a function of instrument temperature in Fig. 13 and as a function of SZA in Fig. 14. In Fig. 13 the fit error increases for temperatures below 10 °C. This can be explained with the variation of the ILF with instrument temperature. The ILF used for the convolution of the Chance and Kurucz (2010) solar atlas spectrum and the absorption cross sections was recorded at room temperature. Pinardi et al. (2007) investigated the change of ILF with temperature and reported variations of the ILF of up to 0.1 nm, in particular at temperatures below room temperature.

In Fig. 14 we can observe that the SO_2 retrieval error largely increases at solar zenith angles above 75°. This behaviour can be caused by a couple of reasons: for one less radiation is available at low SZAs, in particular in the low UV used for the SO_2 evaluation, leading to a poor signal-to-noise ratio. Additionally, low SZAs coincide with lower temperatures, in particular in the morning hours. A third reason can be interferences between O_3 and SO_2 in the DOAS retrieval. Both trace gases have quite similar absorption structures in the UV, large O_3 CDs at large SZAs can lead to non-linearities in the absorption or in the photon light path and thus result in an increased residual structure.

4.4 Relative difference of the SO_2 content from Method A and Method B

Section 4.2 showed that the more commonly applied Method A (removing an SO_2 offset in order to correct for SO_2 contaminated background spectra) sometimes leads to different SO_2 CD than Method B. In order to identify how frequently a significant difference of both methods can be observed, we look at the relative ratio R of the SO_2 CDs determined with the two methods:

$$R = \frac{\overline{S_{SO_2}(B)} - \overline{S_{SO_2}(A)}}{\overline{S_{SO_2}(B)}}, \quad (4)$$

where $\overline{S_{SO_2}(B)}$ is the average SO_2 CD for one scan from Method B and $\overline{S_{SO_2}(A)}$ is the average CD from Method A. Since the slope of the linear fit against the dSCDs of Method B and Method A was not exactly unity (see Sect. 4.3 and Fig. 6), we multiplied the SCDs from Method B with a correction factor (see Table 1). We only averaged over spectra in a scan that exceed a certain SO_2 threshold (for Method B) in order to reduce influences of possible retrieval inaccuracies and to avoid dividing by zero when calculating the relative difference R. Additionally, in order to reduce possible errors due to strong ozone absorption, we only used the following spectra for further investigation:

- Only spectra with an SO_2 CD above 5×10^{17} [molecules cm^{-2}] were taken into account for the averaging process. This ensures a robust relative ratio by preventing divisions with values close to zero in Eq. 4 and reducing the influence of inaccuracies in the retrieval for low SO_2 contents.
- Only spectra with an SZA below 70° were taken into account in order to circumvent potential problems due to strong ozone absorption at lower SZAs.

Figure 15 shows histograms of the relative difference R for Nevado del Ruiz. For Tungurahua the results are shown in Fig. 16. The histogram plots show the relative difference for all data (top left) and for different wind speed intervals in the other plots. Wind speeds were taken from the ECMWF (European Centre for Medium-Range Weather Forecasts, Dee et al., 2011) database. Wind data are obtained from analysed data products from ECMWF at a spatial resolution of 0.75° and a time resolution of 6 h. Data are interpolated to the location of the crater and time of measurement (in this case the original time stamp from the instruments was used).

The distribution of the relative ratio in the top left of Fig. 15 has a peak at 0 (e.g. both methods give the same SO_2 CD) and a tail that goes up to a relative ratio of 100 % (i.e. Method A finds zero SO_2 while Method B finds a significant amount). The other histograms in Fig. 15 show the same as Fig. 15a; however, each histogram only shows data for a specific wind speed interval. For wind speeds above 10 m s^{-1} (Fig. 15b) a dominant peak at a relative ratio of 0 % can be observed with only few values at a higher relative ratio. This means that both methods essentially give the same result. For wind speeds between 5 and 10 m s^{-1} we observe a slight increase of larger relative ratio values (c). For wind

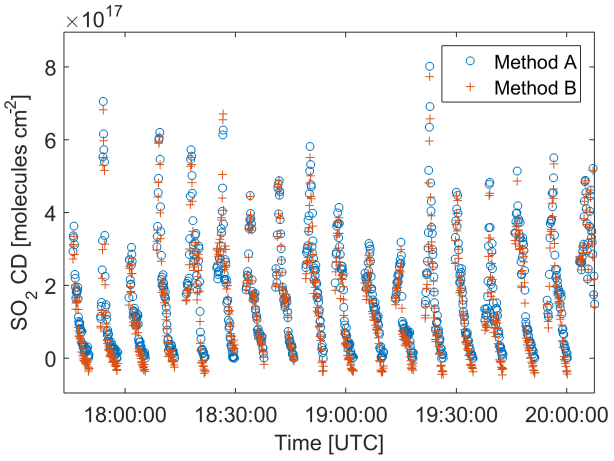

Figure 8. Zoom into the variation of the SO_2 CD at Nevado del Ruiz from instrument D2J2201 on 11 January 2012. In this example both methods agree well.

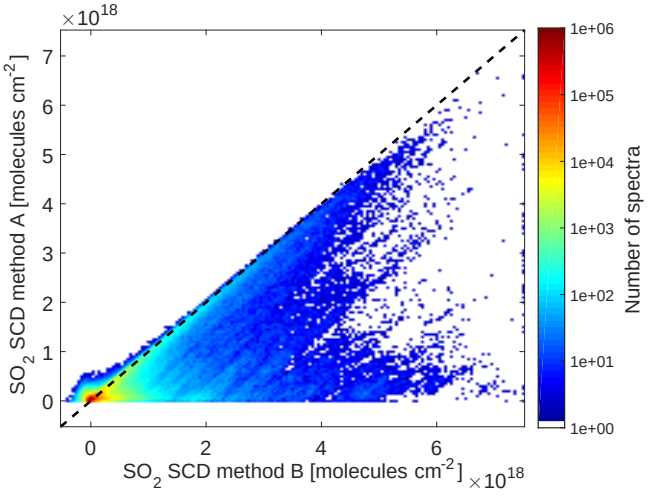

Figure 9. Two-dimensional histogram of the SO_2 SCDs from Method B vs. the SCDs from Method A for instrument D2J2201 at Nevado del Ruiz. Method B, which uses a modelled background spectrum, leads to larger SO_2 column densities. The black-dashed line shows the identity line.

speeds below 5 m s^{-1} (Fig. 15d) we see a homogeneous distribution with almost constant values between 0 and 100 %. This means that we can observe widespread plumes which cover the complete FOV of the scanning-DOAS instrument more frequently at low wind speeds.

When comparing the histograms for Nevado del Ruiz (Fig. 15) and Tungurahua (Fig. 16) we can observe that the relative difference is larger at Nevado del Ruiz. At Nevado del Ruiz 21.4 % of the scans containing significant SO_2 have a relative difference above 0.5, compared to only 7 % at Tungurahua. This indicates that contaminated reference spectra occur more frequently at Nevado del Ruiz. While the relative difference of 0.5 is an arbitrary value, it means only 50 % of absolute SO_2 CD is detected. One possible explanation for the larger number of contaminated spectra at Nevado del Ruiz is the distance of the instruments from the crater (see Table A1). The instruments at Nevado del Ruiz are installed ∼ 3–4 km from the crater, while the instruments at Tungurahua are installed at more than 8 km distance.

5 Conclusions

We developed a new evaluation scheme for volcanic SO_2 relying not on any locally recorded Fraunhofer reference spectrum but rather on a FRS modelled based on a high-resolution solar atlas, which makes the retrieval immune against possibly contaminated reference spectra (i.e. FRS containing absorption structures due to SO_2). Statistical methods were applied in order to identify instrumental effects. Using this evaluation scheme we investigated how frequently contaminated FRS occur for scanning-DOAS instruments from NOVAC at the volcanoes Nevado del Ruiz and Tungurahua.

We observed that the DOAS retrieval, which used the convolved Chance and Kurucz (2010) solar atlas spectrum as FRS, typically showed a similar residual structure for all spectra (before including principal components in the fit). A PCA on the residual structures revealed that the first principal component accounts for more than 88 % of the variation of the residual structures (for all instruments), while the combination of the first two principal components typically accounts for even more than 90 % of the variation. Each of the further principal components only has an individual contribution below 1 % to the residual structure. We interpret the first two principal components as instrumental effects. The first principal component describes the quantum efficiency and grating efficiency of the spectrometer, while the second principal component takes temperature or time-dependent variations into account. However, we cannot completely rule out that these principal components also include structures that are inherent in the Chance and Kurucz (2010) solar atlas as suggested by Burton and Sawyer (2016), which should not affect the fit results. After including the first two principal components as pseudo-absorbers in the DOAS fit we obtained a fit quality comparable to a regular DOAS SO_2 evaluation with an SO_2 DOAS retrieval error as good as 1×10^{16} [molecules cm^{-2}] and typically below 2×10^{16} [molecules cm^{-2}]. The SO_2 fit error shows increased values with low instrument temperatures and high SZA. The temperature dependency of the fit error can be explained by temperature-induced variations of the ILF. Taking these effects into account could further improve the evaluation in the future.

We found that the SO_2 evaluation based on a modelled FRS (Method B) finds the zero level well and that the dSCDs of this method typically lies within 15 % of the dSCDs of a standard DOAS retrieval using an FRS recorded with the same instrument (Method A). Furthermore, the new method

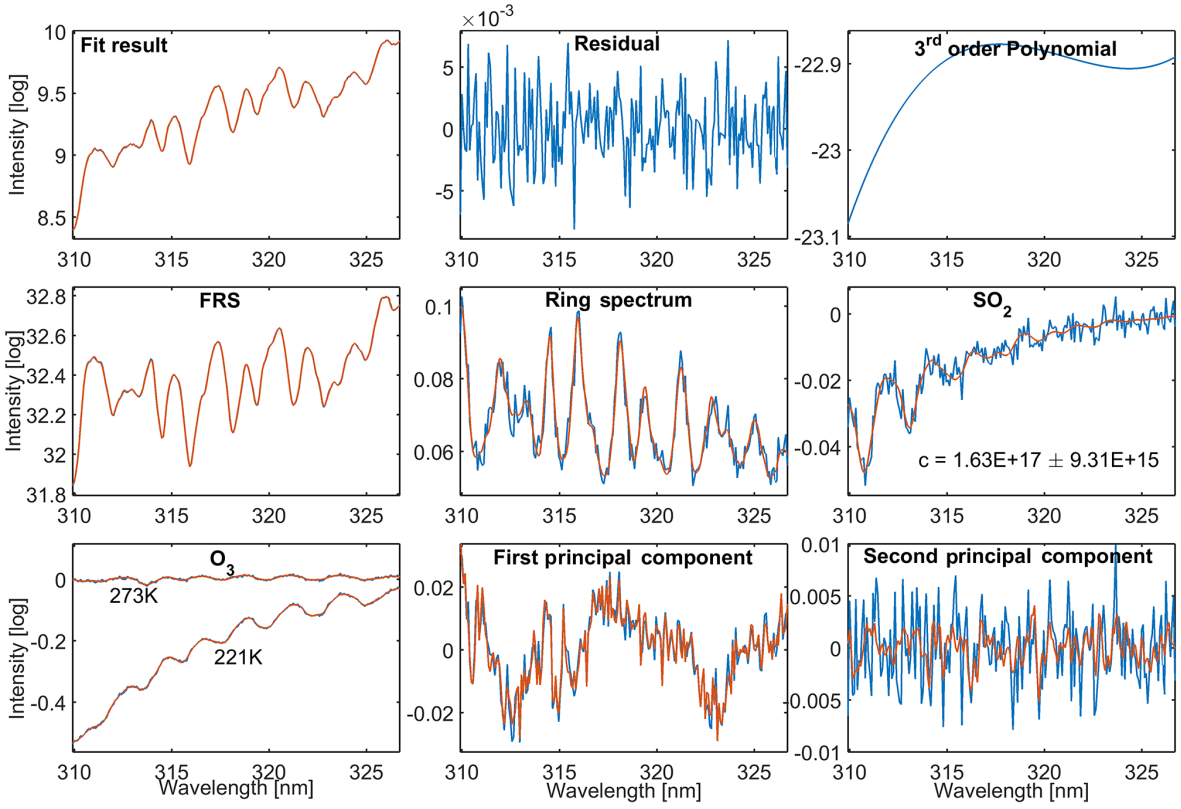

Figure 10. Example SO_2 DOAS fit of instrument D2J2201 (Nevado del Ruiz). The measurement spectrum was recorded on 5 March 2010 at 16:01 (UTC). The model functions are shown in red while the model+the residual (i.e. the measurement) are shown in blue.

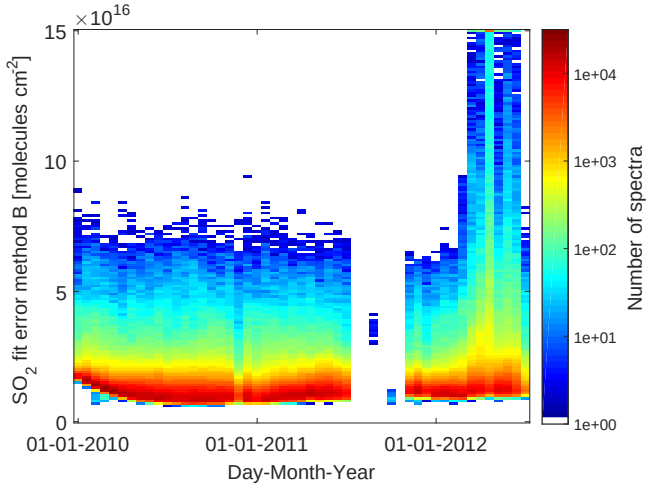

Figure 11. Two-dimensional histogram of the SO_2 DOAS fit error from the solar atlas evaluation as a function time for instrument D2J2201 (Nevado del Ruiz).

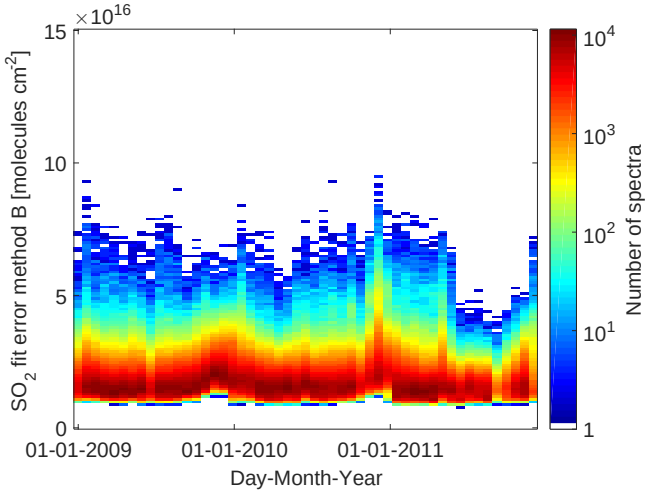

Figure 12. Two-dimensional histogram of the SO_2 DOAS fit error from the solar atlas evaluation as a function time for instrument I2J8548 at Tungurahua.

allows us to retrieve absolute SO_2 CDs. The comparison of the SO_2 CDs of the two methods showed that Method A in a number of cases leads to smaller SO_2 CD values than Method B. We found that at Nevado del Ruiz 21.4 % of the scans containing a significant amount of SO_2 in all viewing directions (according to Method B) show much lower SO_2 CDs for Method A (factor of 2, which corresponds to a relative ratio R; see Eq. (4), of 0.5). At Tungurahua only 7 % of the

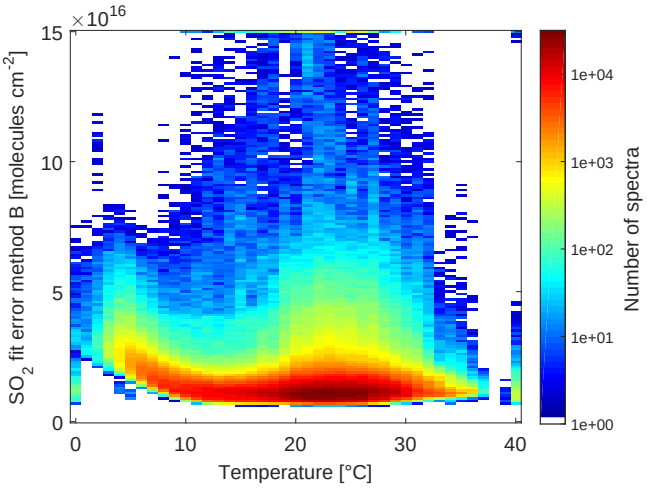

Figure 13. Two-dimensional histogram of the SO_2 DOAS fit error from the solar atlas evaluation as a function of instrument temperature for instrument D2J2201.

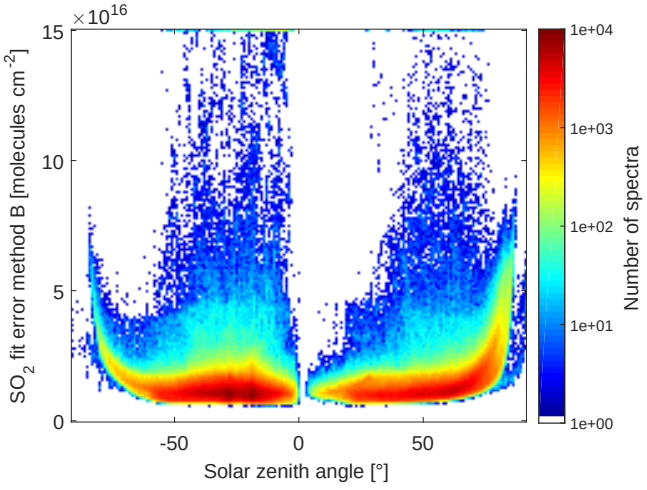

Figure 14. Histogram of the SO_2 DOAS fit error from the solar atlas evaluation as a function of solar zenith angle for instrument D2J2201.

scans have a relative ratio above 0.5. The relative ratio between the two methods shows large values in particular for low wind speeds at both volcanoes. The difference between the two volcanoes might be due to the fact that the stations at Nevado del Ruiz are placed on the flanks of the volcano, at higher altitude and closer to the crater. The enhanced activity and low wind speeds contribute to the occurrence of wide plumes covering all viewing directions of the scanners.

Further validation of the results presented here, e.g. with traverse measurements as in Salerno et al. (2009a), would be advantageous. The authors of Salerno et al. (2009a) found good agreement between their specific FRS evaluation for scanning spectrometers and car traverse measurements at Mt. Etna. However, comparing measurements from such different data sets is complex already for a single volcano, and additional error sources must be taken into account. The observation geometry needs to be controlled in a way that both instruments sample the same section of the plume and are subject to similar radiative transfer effects. The complexity of this can lead to an uncertainty that can be observed in Fig. 6a of Salerno et al. (2009a). Furthermore, the volcanoes studied here are not as easily accessible as Mt. Etna, and regularly conducted traverse measurements cannot be obtained. A direct comparison of the differences observed at the two volcanoes would suffer from additional error sources due to the different set-up locations of the instruments relative to each respective volcano and differences in local meteorological patterns (wind speeds and directions), terrain and subsequent dispersion patterns.

We interpret scans with a large relative ratio between the two methods as situations in which the recorded spectra show signatures of volcanic SO_2 for all viewing directions. Removing an offset value (as for Method A) leads to lower SO_2 CDs and therefore smaller fluxes. It is important to question the reason for signatures of volcanic SO_2 in all viewing directions and what the effect on the SO_2 emission rate retrieval is. There are at least two possible explanations for this phenomenon:

1. It is due to radiative transfer effects; i.e. there is no SO_2 present in the column defined by the instrument viewing direction. However, a fraction of the radiation passed the plume (and thus picked up an SO_2 absorption signature) and then was scattered into the instrument's FOV.

2. There is actually SO_2 in the instrument FOV.

Model calculations to investigate the influence of radiative transfer on SO_2 emission rates at volcanoes were made by Bigge (2015). These radiative transfer model calculations indicate that it is possible to obtain an SO_2 signal in viewing directions that should be gas free according to a geometric approach. This means that radiation passes the volcanic plume before being scattered into the field of view of the spectrometer from a direction that should be gas free. The results of Bigge (2015) showed that the magnitude of these signal depends on the measurement geometry (distance plume instrument, SZA, extent of the volcanic plume). At Nevado del Ruiz the situation gets further complicated, since clouds are present at the volcano almost throughout the entire year. If the difference between methods A and B is caused by a radiative transfer effect, it is difficult to judge which one of the methods leads to more accurate results.

For the second explanation, that actual SO_2 is present in all viewing directions of the particular scan we have to distinguish further between a broadly dispersed (and moving) plume or SO_2 that sits around the instrument without actually moving. The case of an actually broadly dispersed volcanic plume describes a situation in which the volcanic gas plume disperses after being released from the volcano (e.g. due to

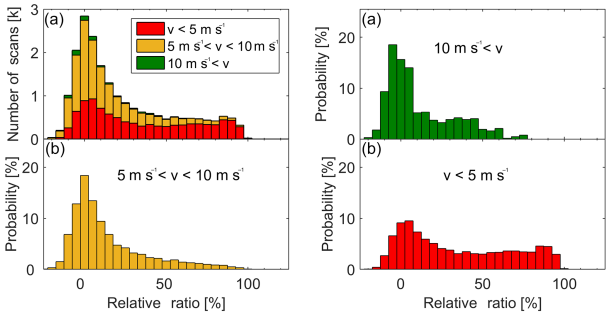

Figure 15. Histograms of the relative ratio $R \times 100\,\%$ (see Eq. 4) between the SO_2 CDs derived by Method A and Method B for different wind speeds at Nevado del Ruiz. The different histograms show the results for both instruments. In the top left the results for all spectra are shown. The top right shows only spectra where the wind speed was above $10\,m\,s^{-1}$. The results for lower wind speeds are shown in the lower part of this figure.

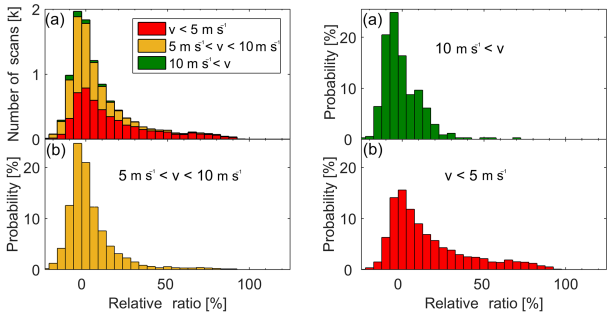

Figure 16. Histograms of the underestimation for different wind speeds at Tungurahua. The results show data from all three instruments.

low wind speeds and thus more time to disperse). In this situation Method A would lead to an underestimation of the SO_2 emission rate, while Method B would give a more accurate picture. However, it is difficult to obtain an SO_2 emission rate from the SO_2 column densities in the case of a dispersed plume with the current integration schemes used in NOVAC since the plume cross section cannot be defined accurately in this situation. Another possibility is that volcanic SO_2 hovers in the vicinity of the instrument (without actually moving). In this (less likely) case Method A would still lead to accurate SO_2 emission rates. Method B would fail to give us a reasonable emission flux since it would add SO_2 that is just sitting around the instrument to the real SO_2 emission rate.

Finally there is the possibility that the SO_2 contamination originates from background SO_2 due to air pollution or other nearby volcanoes. Method A in this case would also would give the more precise result for the SO_2 flux of the volcano under consideration. In summary, however, we believe that a dispersed plume may be the most likely cause for FRS contamination – at least in the cases we investigated – and that the results of Method B give results which are closer to the true SO_2 column density than those of Method A. However, there may be situations in which Method A would in fact provide more correct data. In any case we recommend performing both evaluations in order to have a warning for contaminated FRS.

The approach presented was developed with the aim to implement it into the operational monitoring of spectroscopic networks. Its great advantage is reduction of manual labour (field measurements and calibration) at the expense of a more elaborate statistical evaluation. The main challenge for the implementation is the availability of a "training set" of field-spectra, which is guaranteed to be gas free (the importance of such a data set was also suggested in Burton and Sawyer, 2016). Additionally, the end user has to set a number of instrument-specific parameters, which can potentially influence the performance of the retrieval. These parameters are mainly connected to the PCA and include the χ^2 cut-off value determining which spectra are excluded from PCA, accounting for hot pixels of the detector (which leave a dominant structure in the residual) and a well-chosen number of principal components to include in the DOAS retrieval.

At present, the algorithm can easily be applied to any other volcano of the NOVAC network offline, but it is not yet part of the standard software used by the observatories in the network. The main advantage of implementing this method in the future will be the possibility to identify plume scans not having an SO_2-free spectrum that gives the baseline zero SO_2 level. Currently, lack of a SO_2-free reference spectrum will in some cases result in the standard NOVAC software not calculating the emission rate for such measurements.

In these cases, applying our new method yields the important information that the SO_2 emission rate from the volcano is non-zero if one of the following conditions prevails: (1) the plume is extending at low altitude towards the spectrometer site and/or (2) the plume is elevated but sufficiently extended to fill the entire range of scan angles. Even if those cases only occur rarely at some volcanoes, it is highly advantageous to obtain information on gas emissions in these cases to complement monitored time series. Last but not least, the presented method confirms SO_2 emission rate measurements with low or no degassing present because it eliminates the chance that those are resulting from contaminated FRS.

6 Data availability

Raw spectral data used to obtain the results presented in this study have been acquired within the NOVAC collaboration. Access to these data is permitted with consent of the respective volcanological observatories owning the source instruments, according to their internal policies for data administration. Please refer the author list for contact details.

Appendix A: Calculation of the time offset at Nevado del Ruiz

The instruments at Nevado del Ruiz had minor problems with the GPS antennas, which led to occasionally wrong time stamps in the spectra during complete days. Under the assumption of a constant daily time offset it is possible to identify time offsets with help of a Langley plot of the O_3 CDs. O_3 is mainly distributed in the stratosphere and the light path through the stratosphere largely depends on the SZA. The so-called air mass factor (AMF) can be used to compare the O_3 SCD with the vertical column density (VCD). For small values of the SZA ϑ below 75° the AMF can be approximated by (Platt and Stutz, 2008):

$$\mathrm{AMF} = \frac{1}{\cos(\vartheta)}. \tag{A1}$$

Since the diurnal O_3 VCD variation is small compared to the influence of the SZA, the O_3 SCDs for the morning and evening with the same SZA should be similar. We used this property to determine the time of the instrument. We used the O_3 CD of the O_3 cross section recorded at 221 K from Method B and investigated the Langley plot (a plot of the O_3 SCD as a function of AMF). For correct time settings we observed a smooth line with slight curvature, while for incorrect time settings the Langley plot is not a smooth curve but shows two distinguishable branches for the morning and afternoon.

In order to calculate the time shift we applied a time offset and recalculated the SZAs according to Reda and Andreas (2004)[1]. For each offset value a polynomial of second order was fitted to the Langley plot and the time offset that maximised R^2 was used for this day.

Table A1. Table showing data for the instruments at Nevado del Ruiz and Tungurahua. **(a)** Retrieved SO_2 CDs from Method B, their variation and how many gas-free spectra were taken into account for this statistic. **(b)** Results of a linear fit when plotting Method B – offset vs. Method A (see Fig. 6). **(c)** Comparison the SO_2 DOAS retrieval errors and **(d)** locations of the instrument and statistics on how frequently contaminated spectra exist.

	Volcano	Nevado del Ruiz		Tungurahua		
	station	Bruma	Alfrombrales	Pillate	Bayushig	Huayarapata
	serial number	D2J2200	D2J2201	D2J2140	I2J8546	I2J8548
(a) Gas-free spectra	Mean : SO_2 : CD : S (molecules cm^{-2})	1.0×10^{15}	1.4×10^{15}	-1.8×10^{15}	1.4×10^{15}	-6.9×10^{15}
	$\sigma(S)$ (molecules cm^{-2})	3.6×10^{16}	2.7×10^{16}	3.2×10^{16}	3.6×10^{16}	3.5×10^{16}
	Number of spectra	3.3×10^{5}	3.5×10^{5}	1.8×10^{6}	1.6×10^{6}	2.5×10^{6}
(b) Plot: SO_2 CD (B – offset)	Slope	1.14	0.95	0.91	0.95	0.88
vs. SO_2 CD A	offset (molecules cm^{-2})	-3.0×10^{15}	5.2×10^{15}	7.7×10^{15}	6.8×10^{15}	8.7×10^{15}
(c) Mean SO_2 fit error	Method A (molecules cm^{-2})	1.43×10^{16}	1.38×10^{16}	1.81×10^{16}	1.89×10^{16}	1.89×10^{16}
	Method B molecules cm^{-2}]	1.55×10^{16}	1.46×10^{16}	1.84×10^{16}	1.94×10^{16}	1.85×10^{16}
(d) Statistics	Distance from crater (m)	3100	4150	8000	11900	9100
	Altitude (m a.s.l.)	4865	4500	2550	2750	2850
	Scanner geometry	flat	conical	flat	conical	conical
	Time frame covered (mm/yy)	01/10–06/12	01/10–06/12	01/09–12/11	01/09–11/10	01/09–11/11
	Number of scans	12826	7935	4442	2331	3538
	Relative ratio $\geq 50\,\%$ (%)	22.4	20.0	4.2	7.0	10.0

[1]We used a MatLab implementation of the Reda and Andreas (2004) algorithm by Vincent Roy.

Appendix B: SO_2 CD time series for all instruments

Time series of the SO_2 column density for all instruments are shown in Figs. B1 and B2 (for Nevado del Ruiz) and Figs. B3–5 (for Tungurahua). While Nevado del Ruiz has constantly high activity from the end of 2010, there are different phases with higher and lower activity at Tungurahua.

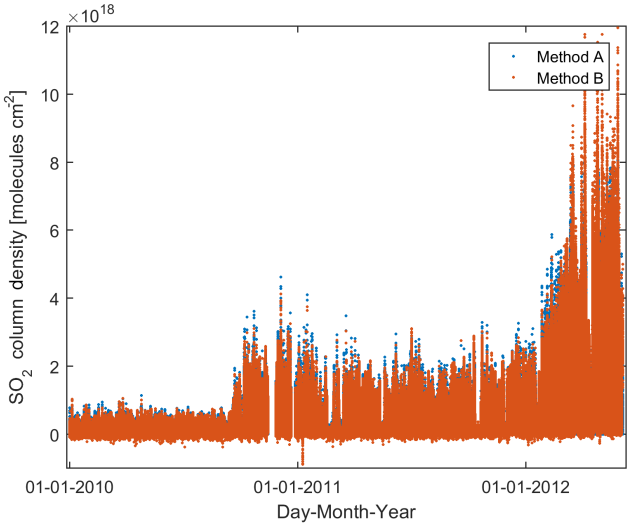

Figure B1. SO_2 CD time series for instrument D2J2200 at Nevado del Ruiz. The blue dots show a NOVAC-type evaluation while the red dots show the SO_2 CDs from a modelled FRS.

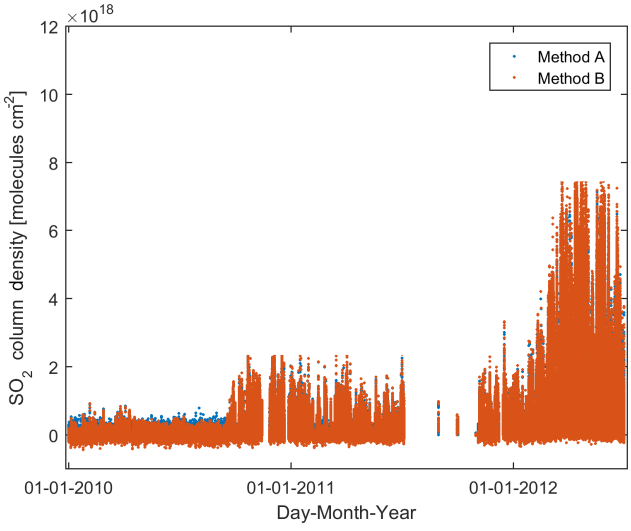

Figure B2. SO_2 CD time series for instrument D2J2201 at Nevado del Ruiz.

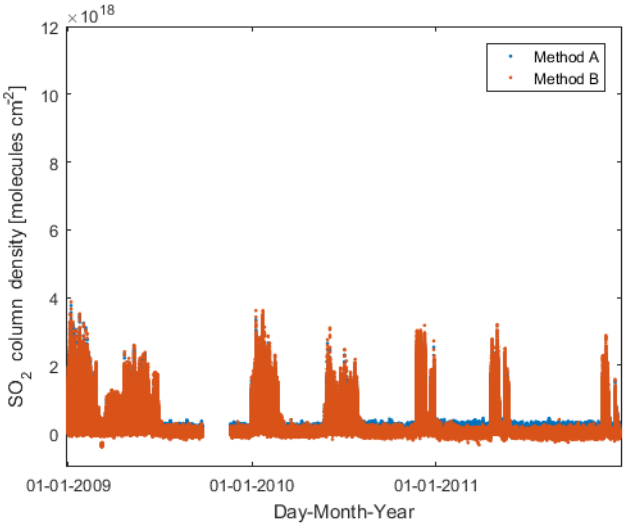

Figure B3. SO_2 CD time series for instrument D2J2140 at Tungurahua. The blue dots show a NOVAC-type evaluation while the red dots show the SO_2 CDs from a modelled FRS.

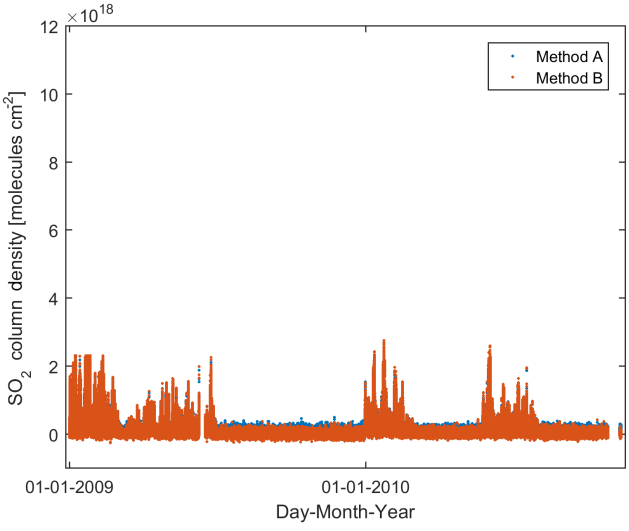

Figure B4. SO_2 CD time series for instrument I2J8546 at Tungurahua.

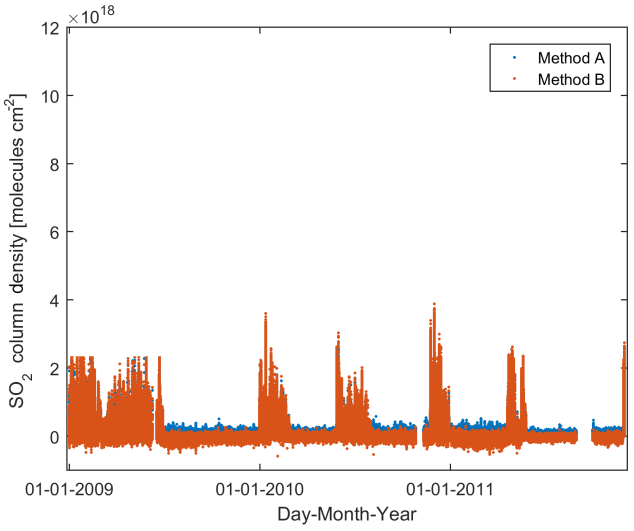

Figure B5. SO_2 CD time series for instrument I2J8548 at Tungurahua.

Appendix C: Implementation of the new algorithm

In summary the evaluation of data in this study encompassed the following steps (which are also shown in Fig. C1):

1. Preparation of the modelled FRS and the gas absorption cross sections:
   a. A gas-free spectrum, recorded with a small SZA, was wavelength-calibrated by comparing it with the Fraunhofer lines of the Chance and Kurucz (2010) solar atlas spectrum. This spectrum was subsequently used as the wavelength grid for this instrument; i.e. all trace gas cross sections and the Ring spectrum were sampled at the wavelength points where this spectrum was sampled.
   b. The Chance and Kurucz (2010) spectrum was convolved using the ILF of the instrument and interpolated to match the wavelength grid from step 1a; this is our modelled FRS for Method B. The Ring spectrum for Method B was calculated from the modelled FRS.
   c. Two O_3 and the SO_2 absorption cross sections were convolved using the ILF of the instrument and the same wavelength grid as above. In order to speed up the evaluation all cross sections were pre-convolved with saturation and I_0 correction using different input SCDs and saved.
2. Spectra were evaluated using two fit scenarios which both use the modelled FRS. The first fit scenario includes the SO_2 cross section; this fit scenario is used to select spectra with negligible SO_2 content for the PCA in Step 3. The second fit scenario does not contain SO_2; it is used to create the residual structures, which are later used in the PCA. After an initial round – to determine estimates of the O_3 and SO_2 CDs for the I_0 and saturation correction – the I_0 and saturation corrected absorption cross sections (from step 1c) were loaded and a second DOAS fit was performed using I_0 and saturation corrected cross sections (the SO_2 CDs and residual structures from these corrected fits were used in Step 3).
3. The residual structures of the DOAS fit (without SO_2 in the fit scenario) were examined using the PCA as described in Sect. 3.3. The spectra which were analysed with the PCA were selected with help of the DOAS fit that included SO_2 (from Step 2).
4. All spectra were evaluated using the DOAS method as described in Step 2 for a second time. This time two different FRS were used. For Method A, a spectrum that was measured with the same instrument directly before the scan (recorded with minimal scan angle) was used as FRS; a Ring spectrum for Method A was calculated from this FRS. All trace gas cross sections (two O_3 as well as one SO_2) were included in the fit. For Method A an offset value was calculated for each scan and subtracted from the SO_2 CDs of each viewing direction (see Sect. 3.2 for details). Method B used the modelled FRS. All trace gas cross sections (O_3 and SO_2) and the first two principal components from Step 3 were included in the fit scenario. For instruments with a hot pixel this was included for Method B as well. I_0 and saturation corrected cross sections were used for Method A and Method B.

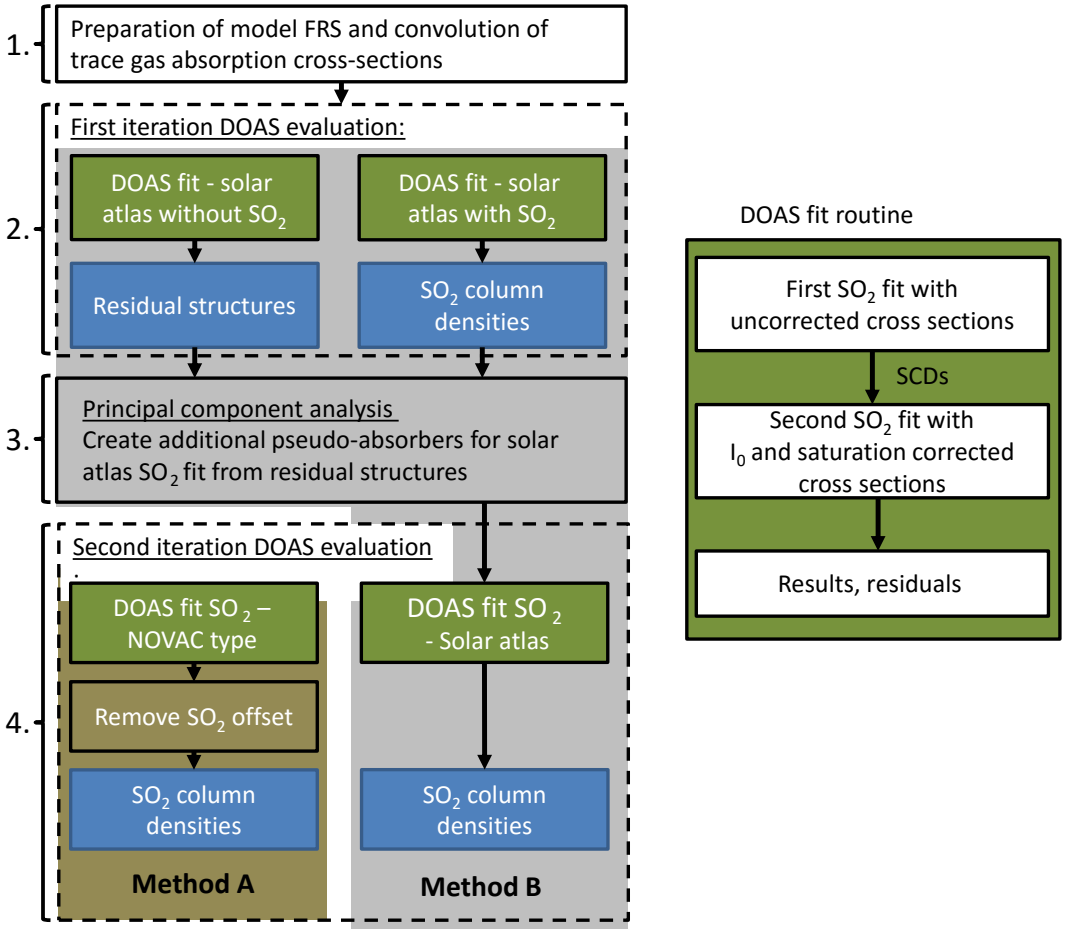

Figure C1. Flow chart of the evaluation steps that were used in order to create the SO_2 column densities from methods A and B.

Appendix D: Variation of the principal components

These figures show the variation of the fit coefficient of the first two principal components for the three instruments that were not shown in the text. Figure D1 shows data for instrument D2J2200 at Nevado del Ruiz while Figs. D2 and D3 show data from instruments D2J2140 and I2J8546, respectively.

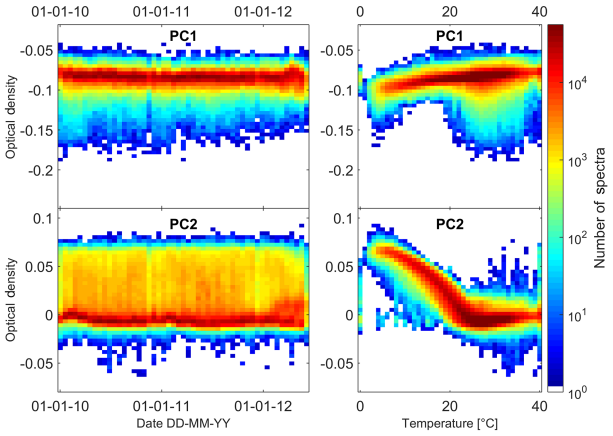

Figure D1. Peak-to-peak apparent optical density (e.g. peak-to-peak optical depth of the principal component times the fit coefficient) of the first and second principal components for instrument D2J2200 at Nevado del Ruiz.

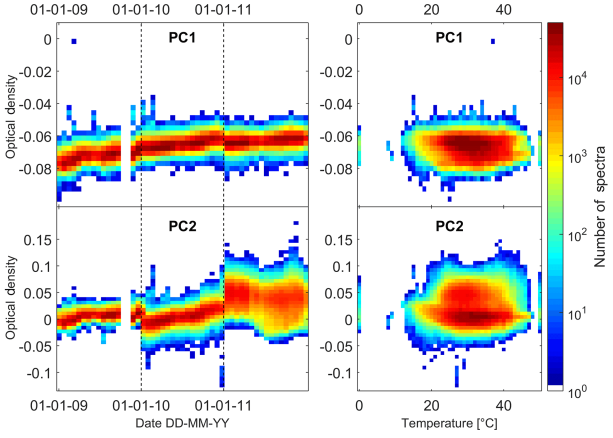

Figure D2. Peak-to-peak apparent optical density (e.g. peak-to-peak optical depth of the principal component times the fit coefficient) of the first and second principal components for instrument D2J2140 at Tungurahua. The vertical dashed lines indicate the start of new time intervals for which a new set of principal components was calculated.

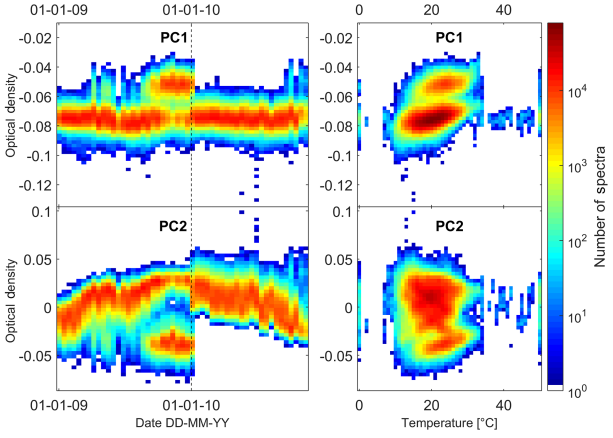

Figure D3. Peak-to-peak apparent optical density (e.g. peak-to-peak optical depth of the principal component times the fit coefficient) of the first and second principal components for instrument I2J8546 at Tungurahua. The two distinct values at the end of 2009 might be due to calibration issues due to a drift of the instrument calibration. Creating the principal components more frequently might help in such cases as can be observed at the beginning of 2010.

Acknowledgements. The authors thank Michel Van Roozendael for editing this paper and Andrew McGonigle, Keith Horton and three anonymous reviewers for their comments on the manuscript. We would like to thank the European Commission Framework 6 Research Program for funding of the NOVAC project. We kindly acknowledge the NOVAC partners from the Colombian Geological Survey (formerly INGEOMINAS), especially the FISQUIM Research Group and the technical staff at the Manizales Volcanological Observatory as well as the staff at Observatorio del Volcán Tungurahua (IGEPN) for keeping the instruments running for almost a decade at Nevado del Ruiz and Tungurahua. Nicole Bobrowski thanks for financial support from DFG BO 3611/1-1 and the VAMOS project. We thank the Deutsche Forschungsgemeinschaft for supporting this work within the project DFG PL193/14-1. We thank the German ministry of education and research (BMBF) for supporting this work within the SOPRAN (Surface Ocean Processes in the Anthropocene) project (Förderkennzeichen: FKZ 03F0662F). Peter Lübcke would like to thank Vincent Roy for providing the MatLab script that was used for calculating the Sun's position.

Edited by: M. Van Roozendael
Reviewed by: A. J. S. McGonigle, D. Horton, and three anonymous referees

References

Bigge, K.: Radiative Transfer in Volcanic Plumes, Master's thesis, Heidelberg University, 2015.

Burrows, J. P., Richter, A., Dehn, A., Deters, B., Himmelmann, S., Voigt, S., and Orphal, J.: Atmospheric remote sensing reference data from GOME2. Temperature dependent absorption cross sections of o_3 in the 231-794 nm range, J. Quant. Spectrosc. Ra., 61, 509–517, doi:10.1016/S0022-4073(98)00037-5, 1999.

Burton, M., Caltabiano, T., Murè, F., Salerno, G., and Randazzo, D.: SO_2 flux from Stromboli during the 2007 eruption: Results from the FLAME network and traverse measurements, J. Volcanol. Geoth. Res., 182, 214–220, doi:10.1016/j.jvolgeores.2008.11.025, 2009.

Burton, M. R. and Sawyer, G. M.: iFit: An intensity-based retrieval for SO_2 and BrO from scattered sunlight ultraviolet volcanic plume absorption spectra, Atmos. Meas. Tech. Discuss., doi:10.5194/amt-2015-380, in review, 2016.

Businger, S., Huff, R., Pattantyus, A., Horton, K., Sutton, A. J., Elias, T., and Cherubini, T.: Observing and Forecasting Vog Dispersion from Kilauea Volcano, Hawaii, B. Am. Meteorol. Soc., 96, 1667–1686, doi:10.1175/BAMS-D-14-00150.1, 2015.

Bussemer, M.: Der Ring-Effekt: Ursachen und Einfluß auf die spektroskopische Messung stratosphärischer Spurenstoffe, Diplomarbeit, University of Heidelberg, 1993.

Chance, K. and Kurucz, R. L.: An improved high-resolution solar reference spectrum for earth's atmosphere measurements in the ultraviolet, visible, and near infrared, J. Quant. Spectrosc. Ra., 111, 1289–1295, doi:10.1016/j.jqsrt.2010.01.036, 2010.

Dee, D. P., Uppala, S. M., Simmons, A. J., Berrisford, P., Poli, P., Kobayashi, S., Andrae, U., Balmaseda, M. A., Balsamo, G., Bauer, P., Bechtold, P., Beljaars, A. C. M., van de Berg, L., Bidlot, J., Bormann, N., Delsol, C., Dragani, R., Fuentes, M., Geer, A. J., Haimberger, L., Healy, S. B., Hersbach, H., Hólm, E. V., Isaksen, L., Kållberg, P., Köhler, M., Matricardi, M., McNally, A. P., Monge-Sanz, B. M., Morcrette, J.-J., Park, B.-K., Peubey, C., de Rosnay, P., Tavolato, C., Thépaut, J.-N., and Vitart, F.: The ERA-Interim reanalysis: configuration and performance of the data assimilation system, Q. J. Roy. Meteorol. Soc., 137, 553–597, doi:10.1002/qj.828, 2011.

Edmonds, M., Herd, R., Galle, B., and Oppenheimer, C.: Automated, high time-resolution measurements of SO_2 flux at Soufrière Hills Volcano, Montserrat, B. Volcanol., 65, 578–586, doi:10.1007/s00445-003-0286-x, 2003.

Elias, T., Sutton, A. J., Oppenheimer, C., Horton, K. A., Garbeil, H., Tsanev, V., McGonigle, A. J., and Williams-Jones, G.: Comparison of COSPEC and two miniature ultraviolet spectrometer systems for SO2 measurements using scattered sunlight, B. Volcanol., 68, 313–322, 2006.

Ferlemann, F.: Ballongestützte Messung stratosphärischer Spurengase mit differentieller optischer Absorptionsspektroskopie, PhD thesis, Heidelberg, Univ., Diss., 1998, 1998.

Galle, B., Oppenheimer, C., Geyer, A., McGonigle, A. J. S., Edmonds, M., and Horrocks, L.: A miniaturised ultraviolet spectrometer for remote sensing of SO_2 fluxes: a new tool for volcano surveillance, J. Volcanol. Geoth. Res., 119, 241–254, doi:10.1016/S0377-0273(02)00356-6, 2003.

Galle, B., Johansson, M., Rivera, C., Zhang, Y., Kihlman, M., Kern, C., Lehmann, T., Platt, U., Arellano, S., and Hidalgo, S.: Network for Observation of Volcanic and Atmospheric Change (NOVAC) – A global network for volcanic gas monitoring: Network layout and instrument description, J. Geophys. Res.-Atmos., 115, D05304, doi:10.1029/2009JD011823, 2010.

Garzon, G., Silva, B., Narvaez, A., Chacon, Z., and Galle, B.: GEOCHANGE: Problems of Global Changes of the Geological Environment, vol. 2, chap. Assessment of SO_2 emissions from three colombian active volcanoes (2007–2012), Science Without Borders, London, 6–14, 2013.

Grainger, J. and Ring, J.: Anomalous Fraunhofer Line Profiles, Nature, 193, 762, 1962.

Hastie, T., Tibshirani, R., and Friedman, J.: The elements of statistical learning, vol. 1, Springer New York, available at: http://statweb.stanford.edu/~tibs/ElemStatLearn/ (last access: 14 November 2016), 2001.

Hibert, C., Mangeney, A., Polacci, M., Muro, A. D., Vergniolle, S., Ferrazzini, V., Peltier, A., Taisne, B., Burton, M., Dewez, T., Grandjean, G., Dupont, A., Staudacher, T., Brenguier, F., Kowalski, P., Boissier, P., Catherine, P., and Lauret, F.: Toward continuous quantification of lava extrusion rate: Results from the multidisciplinary analysis of the 2 January 2010 eruption of Piton de la Fournaise volcano, La Réunion, J. Geophys. Res.-Sol. Ea., 120, 3026–3047, 2015.

Hidalgo, S., Battaglia, J., Arellano, S., Steele, A., Bernard, B., Bourquin, J., Galle, B., Arrais, S., and Vasconez, F.: SO_2 degassing at Tungurahua volcano (Ecuador) between 2007 and 2013: Transition from continuous to episodic activity, J. Volcanol. Geoth. Res., 298, 1–14, doi:10.1016/j.jvolgeores.2015.03.022, 2015.

Kraus, S. G.: DOASIS – A Framework Design for DOAS, PhD thesis, University of Mannheim, 2006.

Lampel, J.: Measurements of reactive trace gases in the marine boundary layer using novel DOAS methods, PhD thesis, University of Heidelberg, 2014.

Li, C., Joiner, J., Krotkov, N. A., and Bhartia, P. K.: A fast and sensitive new satellite SO_2 retrieval algorithm based on principal component analysis: Application to the ozone monitoring instrument, Geophys. Res. Lett., 40, 6314–6318, doi:10.1002/2013GL058134, 2013.

Lübcke, P.: Optical remote sensing measurements of bromine and sulphur emissions, PhD thesis, Heidelberg, Univ., Diss., 2014, available at: http://www.ub.uni-heidelberg.de/archiv/16879, 2014.

Lübcke, P., Bobrowski, N., Arellano, S., Galle, B., Garzón, G., Vogel, L., and Platt, U.: BrO / SO_2 molar ratios from scanning DOAS measurements in the NOVAC network, Solid Earth, 5, 409–424, doi:10.5194/se-5-409-2014, 2014.

McGonigle, A. J. S., Inguaggiato, S., Aiuppa, A., Hayes, A. R., and Oppenheimer, C.: Accurate measurement of volcanic SO_2 flux: Determination of plume transport speed and integrated SO_2 concentration with a single device, Geochem. Geophys. Geosys., 6, Q02003, doi:10.1029/2004GC000845, 2005.

Moffat, A. J. and Millan, M. M.: The applications of optical correlation techniques to the remote sensing of SO_2 plumes using sky light, Atmos. Environ., 5, 677–690, doi:10.1016/0004-6981(71)90125-9, 1971.

Pearson, K.: LIII, On lines and planes of closest fit to systems of points in space, The London, Edinburgh, and Dublin Philosophical Magazine and Journal of Science, 2, 559–572, 1901.

Perner, D. and Platt, U.: Detection of nitrous acid in the atmosphere by differential optical absorption, Geophys. Res. Lett., 6, 917–920, doi:10.1029/GL006i012p00917, 1979.

Pinardi, G., Roozendael, M. V., and Fayt, C.: The influence of spectrometer temperature variability on the data retrieval of SO_2., In NOVAC second annual activity report, 44–48, NOVAC consortium, 2007.

Platt, U. and Stutz, J.: Differential Optical Absorption Spectroscopy – Principles and Applications, Physics of Earth and Space Environments, Springer Berlin Heidelberg, 2008.

Platt, U., Marquard, L., Wagner, T., and Perner, D.: Corrections for zenith scattered light DOAS, Geophys. Res. Lett., 24, 1759–1762, doi:10.1029/97GL01693, 1997.

Reda, I. and Andreas, A.: Solar position algorithm for solar radiation applications, Solar Energ., 76, 577–589, doi:10.1016/j.solener.2003.12.003, 2004.

Salerno, G., Burton, M., Oppenheimer, C., Caltabiano, T., Randazzo, D., Bruno, N., and Longo, V.: Three-years of SO_2 flux measurements of Mt. Etna using an automated UV scanner array: Comparison with conventional traverses and uncertainties in flux retrieval, J. Volcanol. Geoth. Res., 183, 76–83, 2009a.

Salerno, G., Burton, M., Oppenheimer, C., Caltabiano, T., Tsanev, V., and Bruno, N.: Novel retrieval of volcanic SO_2 abundance from ultraviolet spectra, J. Volcanol. Geoth. Res., 181, 141–153, doi:10.1016/j.jvolgeores.2009.01.009, 2009b.

Shefov, N. N.: Intensivnosti nokotorykh emissiy sumerochnogo i nochnogo neba (Intensities of some Emissions of the Twilight and Night Sky), Spectral, electrophotometrical and radar researches of aurorae and airglow, IGY program, section IV, 1, 25, 1959.

Smith, L. I.: A tutorial on principal components analysis, Cornell University, USA, 51, 52, 2002.

Stoiber, R. E., Malinconico, L. L., and Williams, S.: Use of the correlation spectrometer at volcanoes, in: Forecasting volcanic events, edited by: Tazieff, H. and Sabroux, J.-C., Elsevier Science Pub. Co., Inc., New York, NY, 424–444, 1983.

Vandaele, A., Hermans, C., and Fally, S.: Fourier transform measurements of SO_2 absorption cross sections: II.: Temperature dependence in the 29 000–44 000 cm^{-1} (227–345 nm) region, J. Quant. Spectrosc. Ra., 110, 2115–2126, doi:10.1016/j.jqsrt.2009.05.006, 2009.

Wenig, M., Jähne, B., and Platt, U.: Operator representation as a new differential optical absorption spectroscopy formalism, Appl. Opt., 44, 3246–3253, 2005.